Comparison of the Dependence of Blood R_2 and R_2^* on Oxygen Saturation at 1.5 and 4.7 Tesla

M.J. Silvennoinen,[1,4] C.S. Clingman,[1,2] X. Golay,[1,3] R.A. Kauppinen,[1,4] and P.C.M. van Zijl[1–3]*

Gradient-echo (GRE) blood oxygen level-dependent (BOLD) effects have both intra- and extravascular contributions. To better understand the intravascular contribution in quantitative terms, the spin-echo (SE) and GRE transverse relaxation rates, R_2 and R_2^*, of isolated blood were measured as a function of oxygenation in a perfusion system. Over the normal oxygenation saturation range of blood between veins, capillaries, and arteries, the difference between these rates, $R_2' = R_2^* - R_2$, ranged from 1.5 to 2.1 Hz at 1.5 T and from 26 to 36 Hz at 4.7 T. The blood data were used to calculate the expected intravascular BOLD effects for physiological oxygenation changes that are typical during visual activation. This modeling showed that intravascular ΔR_2^* is caused mainly by R_2 relaxation changes, namely 85% and 78% at 1.5T and 4.7T, respectively. The simulations also show that at longer TEs (>70 ms), the intravascular contribution to the percentual BOLD change is smaller at high field than at low field, especially for GRE experiments. At shorter TE values, the opposite is the case. For pure parenchyma, the intravascular BOLD signal changes originate predominantly from venules for all TEs at low field and for short TEs at high field. At longer TEs at high field, the capillary contribution dominates. The possible influence of partial volume contributions with large vessels was also simulated, showing large (two- to threefold) increases in the total intravascular BOLD effect for both GRE and SE. Magn Reson Med 49:47–60, 2003. © 2003 Wiley-Liss, Inc.

Key words: Key words: BOLD contrast; transverse relaxation; fMRI; blood; intravascular

Most BOLD-fMRI studies employ R_2^* contrast changes, which, compared to R_2 changes, are larger and take place both inside the vasculature and in the tissue surrounding the vessels (1,2). Hoogenraad et al. (3) recently provided an overview of these BOLD R_2^* relaxation processes and their roles in different types of experiments and brain regions. Intravascular contributions consist of intrinsic blood R_2^* relaxation, as well as additional dephasing due to susceptibility differences between blood and tissue, or changes in local blood velocity. Extravascular vessel-size-dependent effects due to vessel-tissue susceptibility differences are expected around both capillaries and larger vessels. Susceptibility-based dephasing mechanisms have been modeled (4–6), and based on these theoretical predictions, most in vivo BOLD quantification approaches focus on extravascular R_2^* effects. However, experiments at low and intermediate field strengths have shown that the intravascular contribution of large vessels to the fMRI signal is dominant (2,7–10). When motional weighting with magnetic field gradients is employed (2,11), approximately 60–70% of the R_2^* effect can be removed. Based on flow and diffusion considerations, such experiments remove most signals originating from inside large vessels and from arterioles and venules above 10–20 μm. The total BOLD R_2^* effect is also expected to have a substantial intravascular contribution from venules and capillaries, because R_2 effects in pure blood are very large (12–14). To better understand the origin of the R_2^* BOLD effect, it is important to determine what part of the fMRI changes is of intravascular origin, and how this fraction behaves as a function of oxygen saturation (Y) and hematocrit fraction (Hct). One recent study reported spin-echo (SE) and gradient-echo (GRE) BOLD results as a function of blood oxygenation at 1.5 T (14). In these experiments, R_2^* was derived from the free induction decay (FID) of a multi-SE sequence. The results were surprisingly different from those of multi-GRE in vivo imaging and phantom studies (Table 1) in that they showed a non-Lorentzian behavior instead of a simple exponential decay. The present work reports exponentially decaying multi-GRE measurements in a blood perfusion system, where oxygenation, Hct, and temperature can be controlled and physiological conditions maintained. In addition, SE contributions were measured to assess the relationship between intravascular SE and GRE BOLD changes inside large vessels at two field strengths.

SE and GRE transverse relaxation rates in blood have been studied in detail under many different conditions (12,15–22), and several theories have been proposed for their interpretation. In order to avoid assumption-specific interpretations and to keep the equations as general as possible, we compare only simple features common to all of these experiments. Data have shown that both blood relaxation parameters follow a parabolic behavior as a function of oxygenation saturation fraction Y:

$$R_2 = A + B(1 - Y) + C(1 - Y)^2 \quad [1a]$$

$$R_2^* = A^* + B^*(1 - Y) + C^*(1 - Y)^2 \quad [1b]$$

[1]Department of Radiology, Johns Hopkins University School of Medicine, Baltimore, Maryland.

[2]Department of Biophysics, Johns Hopkins University School of Medicine, Baltimore, Maryland.

[3]F.M. Kirby Research Center for Functional Brain Imaging, Kennedy Krieger Institute, Baltimore, Maryland.

[4]A.I. Virtanen Institute for Molecular Sciences, University of Kuopio, Kuopio, Finland.

Grant sponsor: NIH; Grant number: NS37664; Grant sponsor: NIH/NINDS; Grant number: 31490; Grant sponsor: National Center for Research Resources; Grant number: RR15241; Grant sponsors: Academy of Finland; Maud Kuistila's Memorial Foundation; Finnish Cultural Foundation; Northern Savo Fund; Sigrid Juselius Foundation.

*Correspondence to: Peter C.M. van Zijl, Johns Hopkins University School of Medicine, Dept. of Radiology, 217 Traylor Bldg., 720 Rutland Ave., Baltimore, MD 21205. E-mail: pvanzijl@mri.jhu.edu

Received 29 April 2002; revised 13 August 2002; accepted 21 August 2002.

DOI 10.1002/mrm.10355

Published online in Wiley InterScience (www.interscience.wiley.com).

Table 1
Overview of the Experimental Conditions of R_2 and R_2^* Experiments in the Literature

		Temp, °C	Sequence	Tube	Voxel
Chien et al. (19)	Human, in vitro	37	Imaging (single GRE), TE 9–80 ms	10 ml glass tubes	FOV 250 mm, 1 mm slice
Barth and Moser (40)	Human, in vitro	23	Imaging, multiecho GRE TE 4–500 ms, variable echo delays TR as short as possible	13 mm diameter	1.5 × 1.5 mm^2
Li et al. (22)	Human, in vitro	Not available	Imaging, multiecho GRE TE 9–175 ms, delay 11 ms TR 188 ms		0.63×4 mm^3
Li et al. (22)	Human, in vivo	In vivo	Imaging, multiecho GRE TE 8.6, 30, 50, 70 (art.), 8.6,30,40,50 (veins) TR from cardiac cycle (art.), veins not reported	Femoral artery, vena cava	0.8 × 0.6 × 4 mm^3 (arteries) 1.6 × 1.3 × 4 mm^3 (veins)
Li et al. (22)	Pig, in vivo	In vivo	Imaging, multiecho GRE TE 8.6, 30, 50, 70 TR from cardiac cycle (art.), veins not reported	Descending aorta, vena cava	0.8 × 0.6 × 4 mm^3 (arteries)
Spees et al. (14)	Human, in vitro	37	Spectroscopic, 5 mm slice across the tube. R_2^* analyzed from an FID after CPMG train TR not reported	5 mm NMR tube	10 mm^3
Wright et al. (17)	Human, in vitro	37	Imaging, CPMG SE, 1–4 π pulses, τ_{CPMG} = 6–48 ms, TE = 1.8–2 s, spiral acquisition, no slice selection	5 ml glass tubes	?

in which the rate constants A, B, and C for the constant, linear, and quadratic oxygenation dependence of R_2 and R_2^* are labeled without and with an asterisk, respectively. For R_2, these A, B, and C values have been related to magnetic susceptibilities, as well as to erythrocyte and plasma relaxation rates (23,24). For R_2^* no such theoretical interpretation of the constants A^*, B^*, and C^* has been made to date. The goal of this work is to compare these constants, rather than to interpret them, as a function of oxygenation at several hematocrit values, thereby providing baseline data for the understanding of intravascular BOLD changes for SE and GRE experiments.

METHODS

Sample Preparation

Bovine blood containing 20 mM sodium citrate, at various hematocrit fractions, were prepared by mixing plasma and cells. Samples of 200 ml were circulated in a gas exchange system (18,20) and through the magnet at 37°C (for details see Ref. 24). Blood oxygenation was manipulated using mixtures of N_2 and O_2, each containing 5% CO_2. Blood gases and oxygenation were monitored using a blood gas analyzer (ABL 700; Radiometer Medical, Brønshøj, Denmark). Samples were drawn three times—at the start, middle, and end of a particular oxygenation. The average Y over these three data points was used. No decaying trends due to possible oxygen consumption by blood cells was found. To avoid erythrocyte precipitation, blood was circulated at all times. During measurements, flow was slowed to 3.1 ml/min (6.2 mm/min). Hemoglobin (Hb, Fe^{+2} center) and metHb (oxidized form of Hb, Fe^{+3} center that can not bind oxygen) levels were analyzed; MetHb was never higher than 2.0%.

MRI and MRS

At 1.5 T (Philips ACS-NT), a standard body coil transmitter and surface coil receiver were used. At 4.7 T (GE Omega), a solenoid coil was used as both transmitter and receiver. The sample tube (∅ 12.5 mm) was positioned vertically in both setups. The surface coil was taped on the side of the tube at 1.5 T, and the tube was inside the solenoid at 4.7 T. Tests with this large-diameter tube parallel and perpendicular to the field showed no difference in the results.

Shimming was performed on the fully oxygenated sample and settings not adjusted at different oxygenations to avoid potentially different shimming contributions to the R_2^* measurements. The reason is that we need to measure the susceptibility effect, but not the background gradients as the sample is not moved when oxygenation is changed. Line widths at half peak height were about 1–3 Hz and 10–20 Hz for oxygenated blood at 1.5 T and 4.7 T, respectively. Because shimming remains constant, it only contributes to A^* in Eq. [1b] and is not oxygenation-dependent. A^* depends on spatial position (GRE experiments can be used for field mapping) and is expected to contribute more in vivo (local susceptibility effects at tissue interfaces) than in vitro. R_2 values were measured using single-echo spectroscopy (TE range at 1.5 T: 20–200 ms; at 4.7 T: 10–200 ms for oxygenated blood and 10–100 ms for deoxygenated samples). Voxels were selected using outer volume suppression above and below the middle of the tube. At 1.5 T, R_2^* was measured from the integral across the tube of the GRE profiles for a 10-mm-thick slice (TE = 10–80 ms). To compare measurements using spectroscopy and imaging (profile), R_2 data from some samples at 1.5 T were acquired using both spectroscopic and profile acquisition. As anticipated, the results indicated that the use of

spectroscopy for R_2 is comparable to the use of profile integration. At 4.7 T, a 2-mm slice was used for the relaxation studies, but even for such a thin slice the quality of the GRE profiles at lower oxygenations was insufficient for using the integral of the complete profile, and only the center part of the tube was used. Due to this problem of very short R_2^*, only *Y*-values > 0.45 and TE = 10–40 ms were used for GRE experiments at 4.7 T. Notice that, when spectroscopy is used instead of imaging, this inhomogeneity effect over even small voxels can lead to higher relaxation rates. When imaging is used, the rates are determined per voxel, and relatively homogeneous regions can be integrated. This may be one reason why investigators using FIDs for R_2^* determination often find much higher rates and sometimes non-Lorentzian behavior.

Simulation of Intravascular BOLD Effects in Parenchyma and Large Vessels

Knowledge of relaxation rates of blood as a function of *Y* and *Hct* allows one to estimate the intravascular BOLD contributions in vivo, if the oxygenations of different vascular compartments are known. Venous oxygenation at baseline activity and during visual stimulation can be calculated from typical values for the oxygen extraction ratio (OER) using $(1 - Y_v) = 1 - Y_a + OER \cdot Y_a$ (23), in which the subscripts "*a*" and "*v*" denote arterial and venous, respectively. Using $Y_a = 0.98$ and OER values of 0.38 (25) and 0.25 at baseline and during activation, respectively, the corresponding venous fractions are 0.61 at baseline and 0.73 during activation. The capillary oxygenation fraction is a function of position between the arterioles and venules, and, as an approximation, we assumed an exponential decay in oxygen saturation to determine average capillary oxygenation fractions $Y_c = 0.77$ and 0.85 during baseline and activation, respectively. To obtain data for the same *Hct* at both fields, we determined all rates at a common physiological *Hct* (= 0.41) using linear extrapolation between the measured rates at normal and low *Hct*. To take into account that the microvascular *Hct* is approximately 85% of that for large vessels (26), we used similar extrapolation to determine rates at *Hct* = 0.35.

The normalized fMRI signal intensity in an MRI voxel consists of signal contributions from parenchyma (pure tissue plus microvessels, i.e., about 200 μm or less), some larger vessels, and cerebrospinal fluid (CSF). The extravascular effect of vessels on the BOLD signal in tissue and CSF is not the topic here. The intravascular effect of larger vessels (arteries and veins) enters in the calculations through partial voluming with the parenchyma. Thus, ignoring partial volume contribution by CSF, the effect of which is small (27), we have the total signal

$$S_{voxel} = (I/I_0)_{voxel} = x_{par}S_{par} + x_{vein}S_{vein} + x_{artery}S_{artery}\,, \quad [2]$$

in which the sum over the voxel components, $x_{par} + x_{vein} + x_{artery} = 1$. In a typical GRE experiment, the large-vessel signal contributions can be written as (28):

$$S_j = \frac{1 - \exp(-TR/T_{1,j})}{1 - \cos(FA)\exp(-TR/T_{1,j})}\sin(FA)\exp(-TE/T_{2,j}^*) \qquad j = \textit{artery or vein}\,, \quad [3a]$$

in which FA is the flip angle. SE signals follow a similar equation with T_2 instead of T_2^*. For parenchyma we have four contributions (k = *tissue*, *arteriole*, *capillary*, *venule*):

$$S_{par} = \sum_k x^k \frac{1 - \exp(-TR/T_{1,k})}{1 - \cos(FA)\exp(-TR/T_{1,k})}\sin(FA)\exp(-TE/T_{2,k}^{(*)})\,. \quad [3b]$$

As always, the fractional sum $\sum_k x^k = 1$. When evaluating x^k, it is important to keep in mind that MR reflects water volume and not tissue volume. Thus, the water contents (C) of gray matter and blood should first be calculated in units of ml water/ml tissue. Using the fact that 1 g water is 1 ml, C is related to the density d (g tissue/ml tissue) and the water content w in (g water/g tissue) via:

$$C_{GM} = d_{GM} \cdot w_{GM} = 1.047 \cdot 0.847 = 0.89 \text{ (ml water/ml gray matter)} \quad [4a]$$

$$C_{blood} = Hct \cdot d_{ery} \cdot w_{ery} + (1 - Hct)d_{plas} \cdot w_{plas} = 0.95 - 0.22Hct \text{ (ml water/ml blood)}\,. \quad [4b]$$

The latter equation is based on data of Tagaki et al. (29), Herscovitch and Raichle (30), and references therein, giving $d_{ery} = 1.10$ g/ml, $d_{plas} = 1.03$ g/ml, $w_{ery} = 0.66$ g/g, and $w_{plas} = 0.92$ g/g. The water fractions for the pure tissue and the microvascular compartments are:

$$x^{tissue} = (C_{GM} - C_{blood}^{micro} \cdot CBV_{GM})/C_{GM} \quad [5a]$$

$$x_i^{micro} = x_{blood,i}^{micro} \cdot C_{blood}^{micro} \cdot CBV_{GM}/C_{GM} \quad [5b]$$

in which i relates to the particular microvessel (arterioles, capillaries, and venules), and in which it is assumed that the total water content of gray matter, as reported in the literature (29), includes the microvascular cerebral blood volume (CBV).

To estimate the microvascular BOLD contributions, we employ a parenchymal model outlined previously (23,31) in which the microvessels, consisting of arterioles ($x_{blood,a}^{micro} = 0.21$), capillaries ($x_{blood,c}^{micro} = 0.33$), and venules ($x_{blood,v}^{micro} = 0.46$) constitute CBV. When Eq. [5b] was used to determine blood contents, it was taken into account that microvascular *Hct* is 85% of that for large vessels (26). The CBV values during baseline and functional activity were 0.047 and 0.059 ml blood/ml GM. The baseline CBV value was taken from Leenders et al. (25) and the activation value was calculated from the CBF change corresponding to a typical OER change from 0.38 during baseline to 0.25 during activation (13). When a 5% increase in oxygen metabolism (32) is used, this corresponds to an increase of 57.5% in CBF, from which CBV is calculated using the square-root dependence for cylinders (13). This is within experimental error of the CBV/CBF data reported by Grubb et al. (33). When the blood volume is changed, we assume that the total water content of the voxel does not change.

We also calculated the effects for a 25% increase in oxygen metabolic rate.

Parenchymal T_2 and T_2^* values for gray matter were taken from the literature: 81 ms (34) and 69.4 ms (8) at 1.5 T, respectively; 54.6 ms (from cat (23,35)) and 22.6 ms at 4.7 T, respectively. Assuming similar parenchymal and tissue T_1 values, the baseline tissue T_1 values were taken as 1.0 s at 1.5 T (28) and 1.5 s at 4.7 T (36). The baseline blood T_1 was taken from our phantom study at 1.5 T (1400 ms (27)), and the same blood/tissue T_1 difference (400 ms) was assumed at 4.7 T, leading to a blood T_1 of 1900 ms. Our phantom measurement showed negligible (about 50 ms) oxygenation dependence of T_1 over the oxygen saturation range of interest, in agreement with previous studies (36). When estimating the effect of partial voluming of large veins at shorter TR, inflow effects will play a role in the BOLD effect. In a recent study (27), we determined that such inflow effects in arteries and veins can be described by assigning an apparent T_1 value to such vessels rather than the true T_1. For 1.5 T, this was found to be about 600 ms at baseline and 450 ms during activation. We used these for the partial voluming estimates for large vessels.

RESULTS

Experiments

Figure 1 shows slice profiles (a, c, e, and g) and corresponding relaxation rate profiles (b, d, f, and h) of the GRE and SE signals at 1.5 T at two different oxygen saturations. Although a slice thickness of 10 mm was used, the profiles are of excellent quality for both sequences. When studying relaxation-rate profiles, it should noted that rates measured in a spectroscopy experiment are based on an exponential fit of the integrals of the signal in the SE profiles. Thus, the deviating values seen at the edge of the tube in the R_2 and R_2^* profiles in Figs. 1 and 2 do not contribute significantly in the resulting overall rates. Figure 2 shows slice profiles (a, c, e, and g) and corresponding relaxation rates (b, d, f, and h) at 4.7 T. Despite the use of a 2-mm slice, over which good homogeneity can easily be achieved, the profiles are worse than at 1.5 T, especially for the GRE signal. This is still true at full oxygenation. Data from a sample tube with an additional narrow tube with flowing blood inside (i–l) show even more deteriorating GRE profiles, but still quite clean SE profiles. Thus R_2^* measurements at 4.7 T have a much larger standard deviation than the R_2 data, even in the more signal-rich, well-shimmed center of the homogeneous measurement tube (Fig. 2a, b, e, and f).

Contrary to results of Spees et al. (14), both SE and GRE data could always be fitted exponentially as a function of TE to determine the relaxation rates. These R_2 and R_2^* values were subsequently fitted as a parabolic function of Y (Eqs. [1a] and [1b]). Figure 3 and Table 2 show R_2, R_2^*, and $R_2' = R_2^* - R_2$ for three different *Hct* values at 1.5 T (Fig. 3a–c) and 4.7 T (Fig. 3d–f). As indicated by Wright et al. (23), the B and C constants in such parabolic fits may compensate each other, leading to meaningless variations in B and C. We therefore also fitted all data with only two constants: a non-oxygenation-dependent (A) and a quadratic (C) one (Table 2). This two-parameter approach also provided excellent fits, well within experimental error of the data (R^2-value higher than 0.95 for all fits at 1.5 T, and 0.81–0.99 for fits at 4.7 T). In general, R^2-values for low hematocrit data were better than for high *Hct*. The R^2 of *AC* fits was at least 85% (*Hct* 0.75, SE at 4.7 T), but in most cases over 99% of R^2 for *ABC* fits. Finally, R_2^* data were

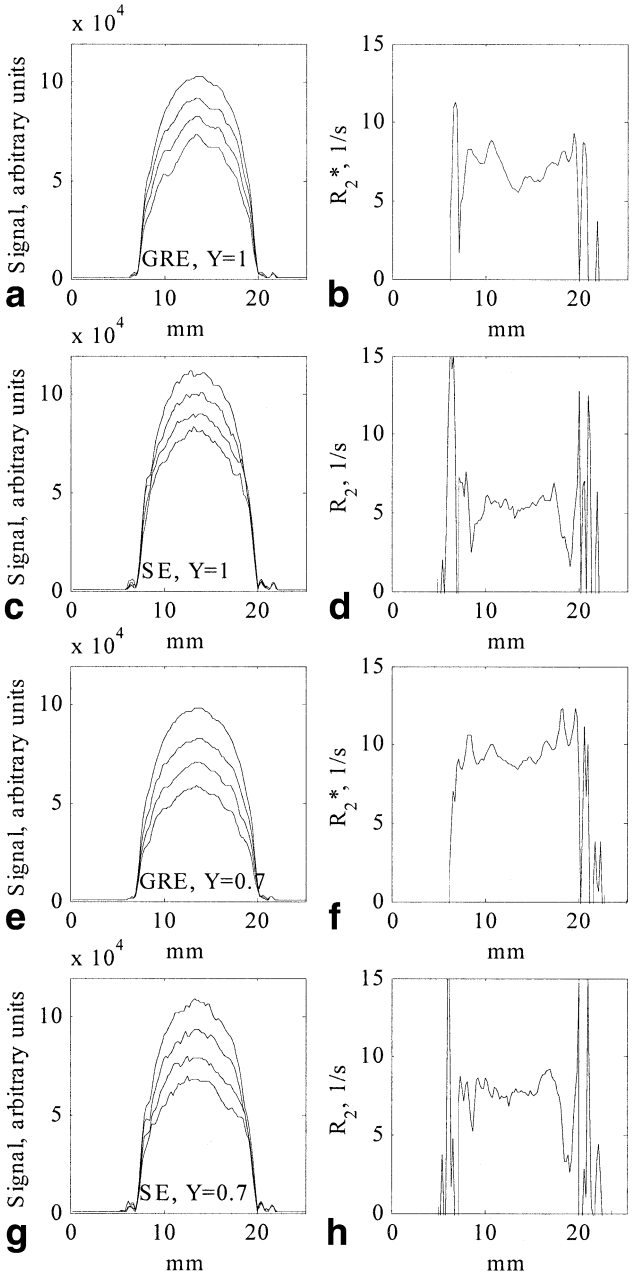

FIG. 1. Slice profiles (**a**, **c**, **e**, and **g**) and corresponding transverse relaxation rate profiles (**b**, **d**, **f**, and **h**) for two oxygenations (**a–d** and **e–h**) at 1.5 T. The four slice profiles per graph correspond to four TEs. Data were acquired from a 10-mm slice. Note that R_2 measured in a spectroscopy experiment will be reflected by the R_2 profile weighted by the signal contributions as a function of position in the tube. Thus, the deviating values at the edge of the tube, because of low SNR due to little signal at the edges, do not contribute significantly to the data in the tables.

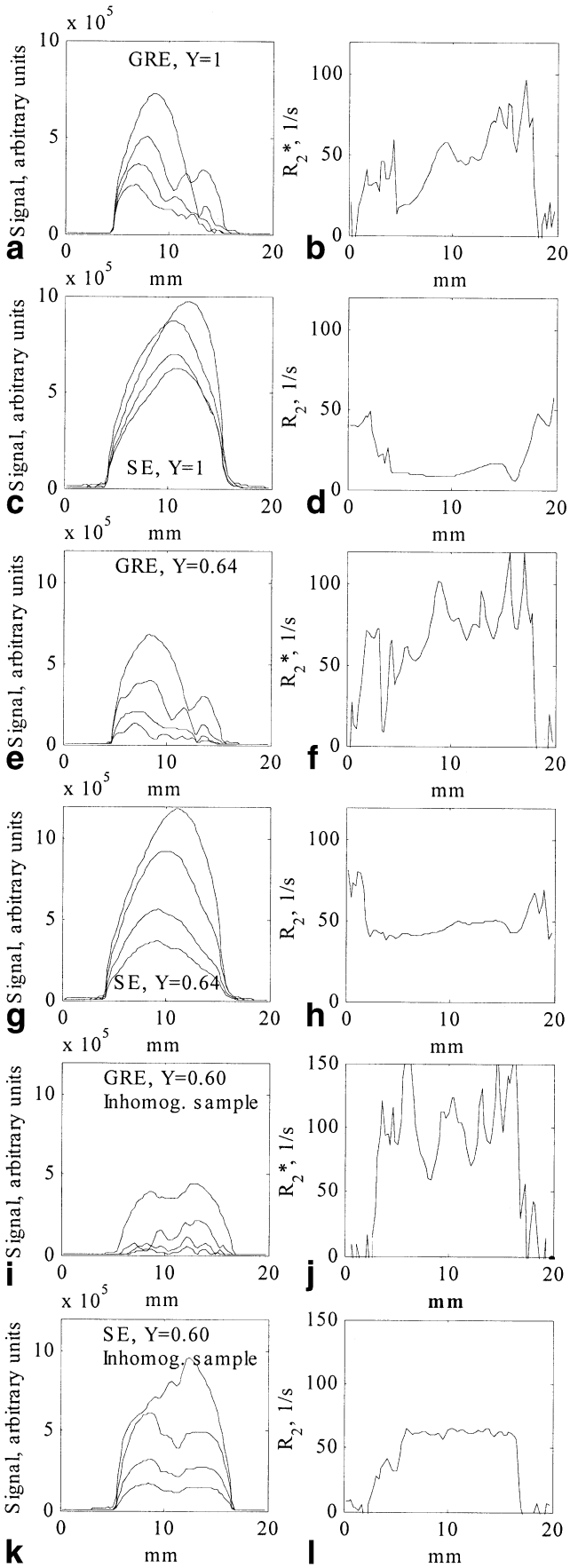

FIG. 2. Slice profiles (**a**, **c**, **e**, and **g**) and corresponding transverse relaxation rate profiles (**b**, **d**, **f**, and **h**) for two oxygenations (**a–d** and **e–h**) at 4.7 T. The four slice profiles per graph correspond to four TEs. Data were acquired from a 2-mm slice through the homogeneous sample tube used to acquire the data in Fig. 3. **i–l:** Data from a 2-mm slice through a sample tube with a narrow tube inside it show deteriorating GRE profiles, but quite clean SE profiles. As explained in the legend of Fig. 1, the R_2 values measured at the tube edges are due to the low signal at the edge of the tubes and do not reflect measurement accuracy for the data in the tables, as they do not contribute significantly to the integral over the curve, which is weighted by the amount of signal.

also fitted using the *B*- and *C*-values for the R_2 curve, to test whether, within experimental error, the changes in R_2 and R_2^* upon oxygenation have an equivalent origin. These fits, however, were only satisfactory for the lowest *Hct*-values and thus were not included here. We also calculated ΔR_2 and ΔR_2^* values at baseline activity and during visual stimulation using the parabolic constants from the two-parameter fit. The resulting numbers (Table 2) show that the blood BOLD changes as a function of oxygenation at 4.7T are dominated (about 80%) by the R_2 contributions for the physiological range in vivo both at 1.5 and 4.7 T.

Simulations

We used the experimental data to calculate R_2 and R_2^* at both fields for $Hct = 0.41$ (large vessels) and $Hct = 0.35$ (microvessels). Using the relaxation times for gray matter in vivo, it is then possible to estimate intravascular BOLD changes for pure parenchyma (tissue + microvessels) and for parenchyma with large vessel contamination. As these predictions depend on the chosen experimental parameters, especially the partial volume fractions for the different voxel compartments, the results can vary strongly. Because most investigators are interested in relative changes, we calculated (Fig. 4) the intravascular percentual BOLD changes for pure veins, pure parenchyma, and parenchyma with minor partial voluming with large veins (2%) and arteries (0.8%). Table 3 lists the results for frequently-used TE and TR values in vivo (FA = 90°). At 1.5 T, for the TE range shown, the relative BOLD changes for both SE and GRE keep increasing monotonously as a function of TE for parenchyma and parenchyma slightly contaminated by large vessels. In contrast, at 4.7 T, the relative BOLD changes level off for parenchyma, after which they decrease again. This leveling off occurs at shorter TE and the postleveling decrease happens at higher rate for parenchyma that is contaminated with veins. For SE, the maximum is at about $TE = T_2 = 55$ ms; for GRE it is around 40–50 ms, which is at $TE > T_{2par}^*$ (= 23 ms). Another interesting observation is that at 1.5 T, relative intravascular GRE-BOLD is larger than SE-BOLD, while at 4.7 T the relation is inverted. The effects for a 25% increase in oxygen metabolism together with the 57.5% change in CBF are also given in Table 3. Notice that a lesser mismatch between oxygen metabolism and CBF reduces the BOLD effect, as BOLD changes are only possible because of this mismatch (23). However, the shape of the

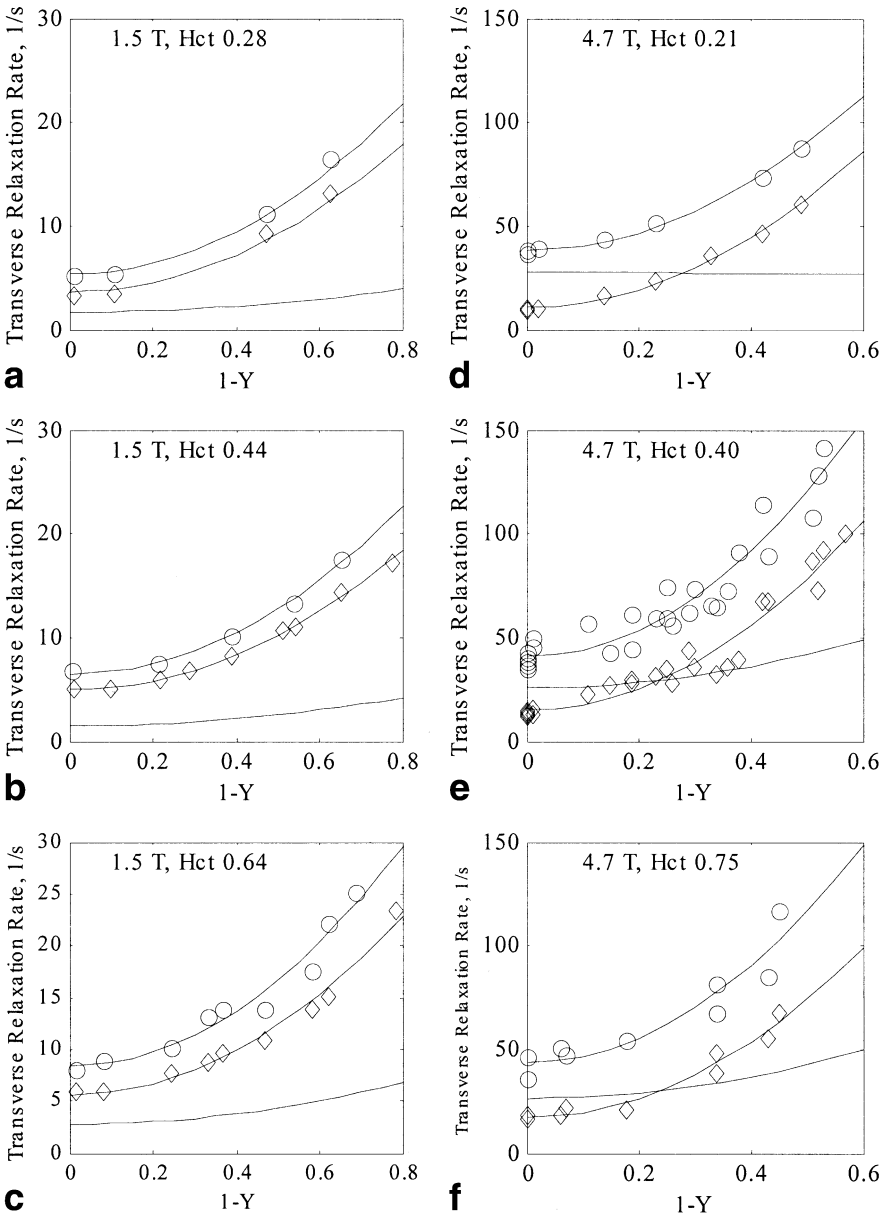

FIG. 3. Transverse relaxation rates R_2 (diamonds), R_2^* (circles), and R_2' (no markers) at 1.5 Tesla (**a–c**) and 4.7 T (**d–f**) as a function of oxygenation fraction (*Y*) for three different *Hct* values. Fits of the data are with a second-order polynomial, the constants of which are given in Table 2.

TE dependence did not change much, except for a small shift of the maximum response at high field to lower TE.

To better understand the contributions of the individual microvessels to the parenchymal changes, we plotted these in Fig. 5. It can be seen that at 1.5 T the venous contribution is larger than the capillary one, which is again larger than the arterial one. At 4.7 T, this same behavior is seen at short TE, but changes drastically at longer TE, where the capillary contribution dominates the BOLD signal change. The reason for this reduced venous contribution to the BOLD effect is not the magnitude of the venous BOLD effect (very large at high field), but the short transverse venous relaxation rate, which reduces the signal contribution. Figure 6 shows the relative signal contribution of the individual microvascular compartments and the total microvasculature response, normalized to the parenchymal signal at each TE. Note that the intravascular venous contribution to the total signal increases with TE at low field and reduces with TE at high field, where the arterial signal contribution becomes dominant due to its smaller R_2 and R_2^*.

DISCUSSION

Several conclusions can directly be drawn from the data in Figs. 1–4. First of all, quantification of the BOLD R_2^* effect becomes much more difficult at higher magnetic field strength. The origin of this effect could be based on cellular susceptibility as well as sample tube susceptibility considerations. At higher field, the effect of the susceptibility change from blood to tube walls and air increases. However, distortions in the profiles do not concentrate on the edges of the tube, but rather produce humps in the overall profile. The effects of shimming are expected to be visible in R_2^* profiles, but these should not increase with deoxygenation, because shimming was kept unchanged.

Table 2
Parabolic Constants (in s^{-1}) of Fits of the Relaxation Rates R_2 and R_2^* as a Function of Oxygenation Fraction Using Eqs. [1a], [1b]†

	A	B	C	A*	B*	C*		
1.5 Tesla								
Hct 0.28	3.4	6.1	15	4.8	5.1	20		
Hct 0.44	4.8	1.7	19	6.9	−3.7	30		
Hct 0.64	6.2	−1.5	27	8.6	−1.6	35		
4.7 Tesla								
Hct 0.21	9.7	23	164	38	18	171		
Hct 0.40	15	4	246	42	−17	350		
Hct 0.75	18	−23	278	44	−11	317		
	A	B = 0	C	A*	B* = 0	C*	ΔR_2 (act) s^{-1}	ΔR_2^* (act) s^{-1}
1.5 Tesla								
Hct 0.28	4.0	0	23	5.4	0	26	−1.8	−2.1
Hct 0.44	5.0	0	21	6.5	0	25	−1.7	−2.0
Hct 0.64	5.9	0	25	8.4	0	33	−2.0	−2.6
4.7 Tesla								
Hct 0.21	11	0	210	38	0	206	−17	−16
Hct 0.40	15	0	254	41	0	319	−17	−27
Hct 0.75	17	0	228	44	0	293	−18	−27

†See Figs. 3, 4. Changes in venous rates (s^{-1}) during activation are also calculated for Y changing from 0.61 to 0.73.

However, the spatial quality of GRE data at low oxygenation, especially at 4.7 T, is poorer than for the SE data, rendering their interpretation more difficult. This behavior is probably even more pronounced in vivo, where many macroscopic and microscopic susceptibility differences complicate shimming. To illustrate such effects, we included data from a sample tube with an additional narrow tube with flowing blood inside it (Fig. 2i–l), which dem-

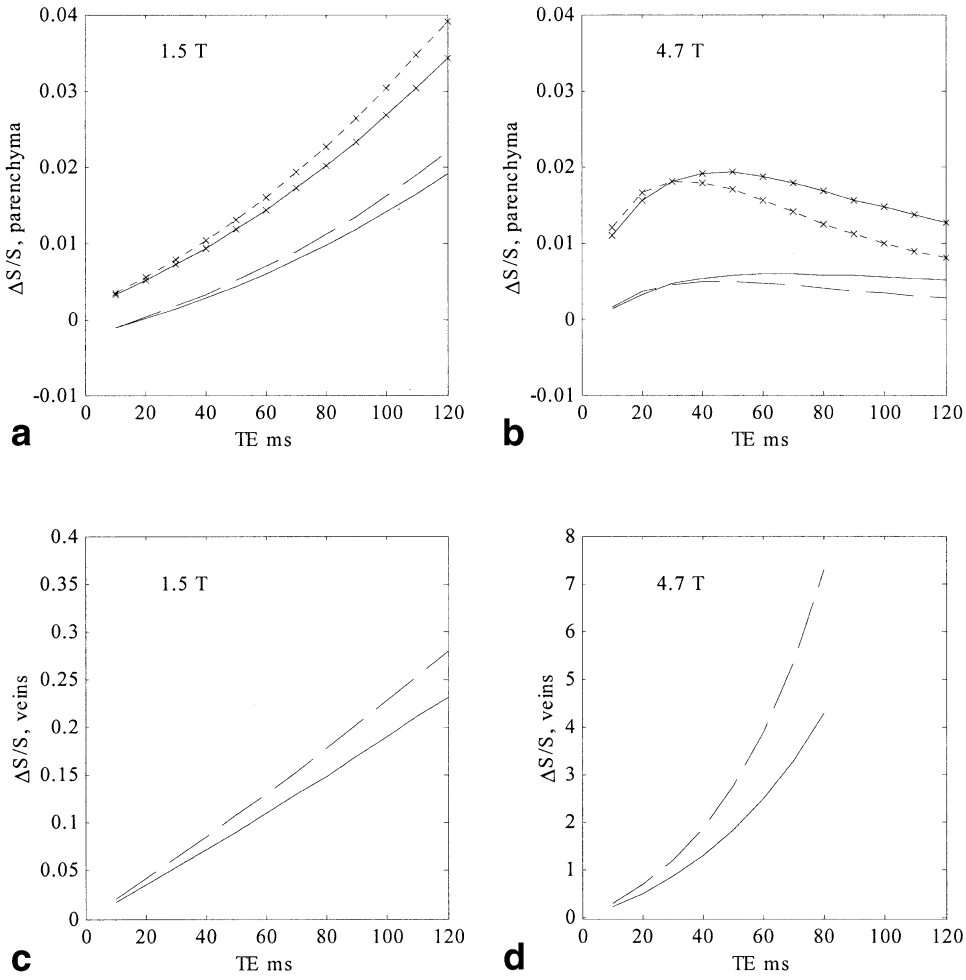

FIG. 4. Estimated SE (solid line) and GRE (dashed line) intravascular relative BOLD signal changes during activation as a function of TE for (**a** and **b**) parenchyma and (**c** and **d**) veins. In **a** and **b** lines without symbols denote pure parenchyma, while lines with cross symbols describe parenchyma with partial volume contributions of 2% veins and 0.8% arteries. Data are given for 1.5 T and 4.7 T using TR = 1 s and FA = 90.

Table 3
Estimated Intravascular Relative BOLD Signal Changes (Hct = 0.41) at Commonly Used Echo Times for Parenchyma, Veins, and Parenchyma With Partial Volume Contributions of Veins (2%) and Arteries (0.8%) at 1.5T and 4.7 T.*

5%/57.5%		Parenchyma		Vein		Parenchyma + partial volume	
		TR = 1s	TR = 3s	TR = 1s	TR = 3s	TR = 1s	TR = 3s
1.5 Tesla							
TE = 50ms	GRE	0.50%	0.75%	11%	11%	1.3%	1.0%
	SE	0.43%	0.66%	9.1%	9.1%	1.2%	0.89%
TE = 80ms	SE	0.96%	1.3%	15%	15%	2.0%	1.7%
4.7 Tesla							
TE = 20ms	GRE	0.36%	0.50%	70%	70%	1.7%	1.2%
	SE	0.33%	0.47%	52%	52%	1.6%	1.1%
TE = 50ms	SE	0.57%	0.73%	180%	180%	1.9%	1.5%
25%/57.5%		**Parenchyma**		**Vein**		**Parenchyma + partial volume**	
		TR = 1s	TR = 3s	TR = 1s	TR = 3s	TR = 1s	TR = 3s
1.5 Tesla							
TE = 50ms	GRE	0.37%	0.60%	7.0%	7.0%	1.1%	0.78%
	SE	0.32%	0.54%	5.9%	5.9%	0.96%	0.69%
TE = 80ms	SE	0.75%	1.00%	9.7%	9.7%	1.6%	1.3%
4.7 Tesla							
TE = 20ms	GRE	0.04%	0.09%	42%	42%	0.93%	0.55%
	SE	0.05%	0.16%	32%	32%	0.93%	0.53%
TE = 50ms	SE	0.07%	0.19%	100%	100%	0.91%	0.59%

*The percentage ratio on the top left indicates the assumed changes in oxygen metabolism and CBF.

onstrated badly deteriorated GRE profiles. Relaxation time profiles confirm these data, showing large fluctuations in R_2^* even in the homogeneous part of the tube that contributes the bulk of the water spins. On the other hand, R_2 data provide a consistently well-shaped profile as a function of position, even under the more severe conditions with two tubes. We therefore conclude that the accuracy of the R_2^* quantification is compromised at higher fields, and that BOLD quantification efforts at such field strengths should probably focus on R_2 determinations. Although total SE-BOLD effects are smaller by about a factor of 3 than R_2^* effects, use of SEs instead of GREs should be well possible at higher fields due to the more-than-linear field dependence of BOLD in venous blood (see ΔR_2^* and ΔR_2 in Table 2). Such a use of SEs at high field was recently demonstrated (37). SE-BOLD is also more simple from a modeling point of view, as a large fraction of the effect can be assumed to be intravascular (1,23). However, care has to be taken with such modeling, because the extravascular R_2 contribution will increase at higher fields (38).

A second important conclusion is that the oxygenation dependence of the BOLD effect in the physiological range ($0 \leq (1 - Y) \leq 0.4$) is very similar for R_2 and R_2^* at both 1.5 T and 4.7 T. At the normal *Hct* of 0.4, values of $R_2' = R_2^* - R_2$ increased only slightly with reduced oxygenation at both fields (Fig. 3). The calculated intravascular BOLD activation effects (Table 2) for a typical venous oxygenation change ($Y_v = 0.61–0.73$) show that BOLD R_2^* changes are dominated by the R_2 contributions at both field strengths. This is in good agreement with data on human activation measured inside venous vessels (10) at 1.5 T, where changes in R_2^* upon visual activation are on the order of magnitude of those measured for R_2 (13,24).

Experimental Considerations

To better judge the validity of our results, we compared the measured venous relaxation rates with available in vitro and in vivo data from the literature (Table 4, Fig. 7). The data in Table 4 show great variation due to various experimental conditions and setups (Table 1). The results for R_2 at physiological *Hct* compare quite favorably, the measured single-echo rate being somewhat larger than values reported for Carr-Purcell-Meiboom-Gill (CPMG) experiments. CPMG data agree well with the data of Golay et al. (24) and Wright et al. (17). These data also support the notion that interspecies (bovine (24) and human (17)) variance between large mammals is not a significant factor in blood relaxation. The 1.5 T R_2^* data in the literature (Fig. 7) range from 5 to 12 s^{-1} for physiological *Y*-values, except for the study by Spees et al. (14), who found twofold greater value as calculated from the parabolic constants for single exponential decay of the FID. Note that the venous R_2^* value of about 10 s^{-1} at 1.5 T is slower than the tissue relaxation rate, a situation that inverts at 4.7 T. The data in Fig. 7 show an increased range of possible R_2^* values at venous oxygenation, which is not unexpected in view of the inherent nature of this parameter. It is sensitive to global field inhomogeneities, which are determined by the particular shim settings and construction details in vitro and by local field variations in tissue, especially at tissue interfaces (CSF, veins, and parenchyma). In addition, in studies of isolated blood, experimental details such as temperature, pulse sequence (spectroscopic vs. imaging, resolution, range of TE values, use of single or multiple echoes) and cell precipitation in the sample during the experiment may have an effect on R_2^*. Hematocrit has been

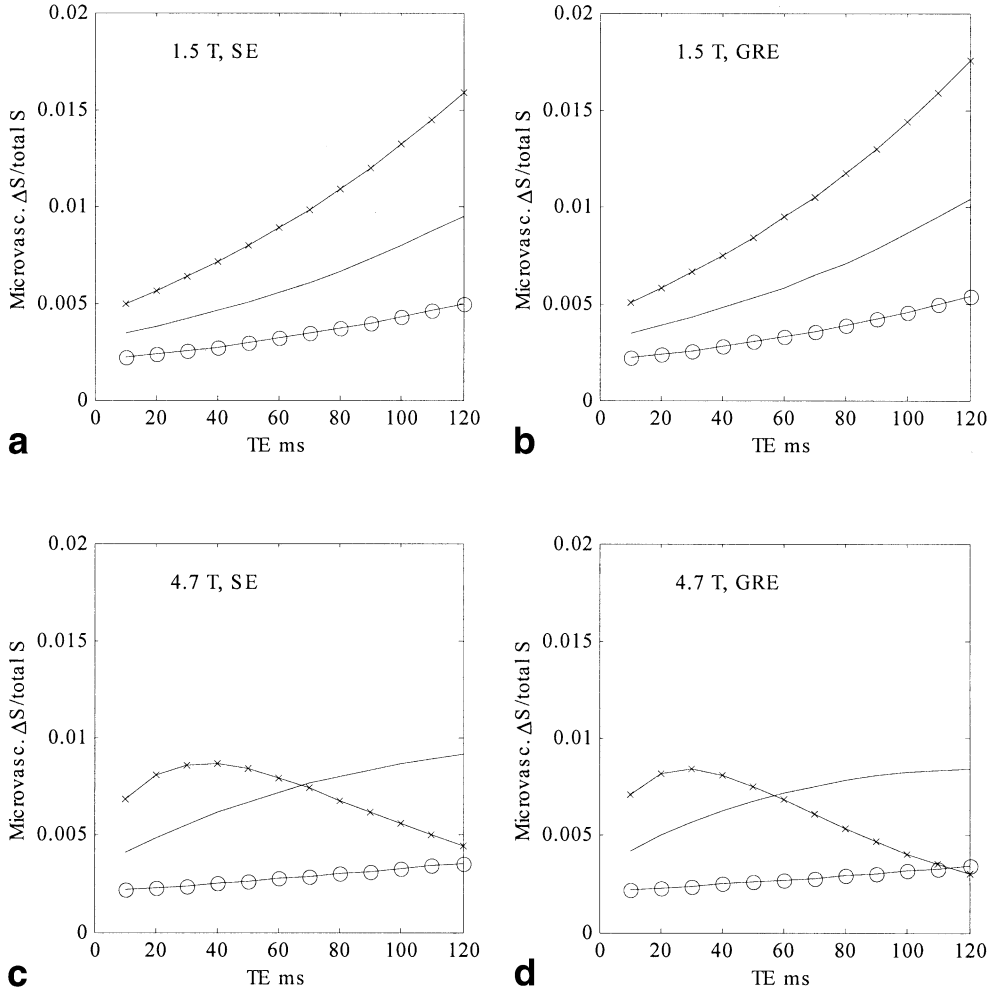

FIG. 5. Estimated relative BOLD signal changes during activation as a function of TE for the individual microvascular compartments (venules: crosses; capillaries: no markers; arterioles: spheres). Signal changes were normalized to the net baseline signal of parenchyma at each TE. Note the reduced influence of the venules and increased contribution of the capillaries at long TE at high field.

shown to affect R_2 relaxation (12,24), and the same is true for R_2^* (Table 2). Temperature can affect relaxation through several mechanisms. First, water diffusion varies with temperature, altering the time scale of motion inside and near the cell, in turn affecting the dephasing rate. Second, cell membrane properties, such as permeability, are temperature-dependent, also affecting water motion (39). Third, temperature influences the kinetic properties of macromolecules, affecting relaxation pathways involving those molecules. Therefore, in Table 4, we compare our data only with those of in vivo studies and in vitro studies conducted at 37°.

Simulations

The present experiments do not provide additional clues about the mechanism of the in vivo BOLD effect. The increase in relaxation rates at lower oxygenation and higher field may result from both intra- and extravascular field-gradient related relaxation mechanisms (2,4,5,12,21), and an exchange-based intravascular mechanism may contribute as well (23). However, the data help provide a better understanding of the intravascular contribution to SE and GRE BOLD effects at different field strengths. For instance, the signal contributions of the different types of vasculature can be evaluated as a function of TE. The simulations in Fig. 4 and Table 3 show that intravascular relative BOLD signal changes in parenchyma increase more than linearly as a function of TE for both R_2 and R_2^* at 1.5 T. At 4.7 T, however, a maximum becomes visible at TE = 40–50 ms for R_2^* and TE = 55 ms for R_2. This maximum is around TE = $T_2(tissue)$ for the SE, but at about TE = $2T_2^*(tissue)$ for the GRE. Interestingly, these maxima become more pronounced and move to lower TE when partial voluming with large vessels is introduced. This partial volume contribution increases at shorter TR and higher field. Large-vessel contamination effects are more pronounced at short TR because inflow effects were taken into account. The increased partial volume effect at high field is due to the fact that venous BOLD changes increase much faster with field than parenchymal changes. This effect is most pronounced at short TE, where an increase by a factor of 4–5 in the relative BOLD effect is predicted. This increase in partial volume contributions at reduced TE seems somewhat puzzling in view of the continuous increase in the relative venous BOLD changes as a function of TE at both high and low fields (Fig. 4c and d). However, this relative increase is somewhat misleading, because the high venous R_2 and R_2^* cause the venous signal contribution to drop off strongly

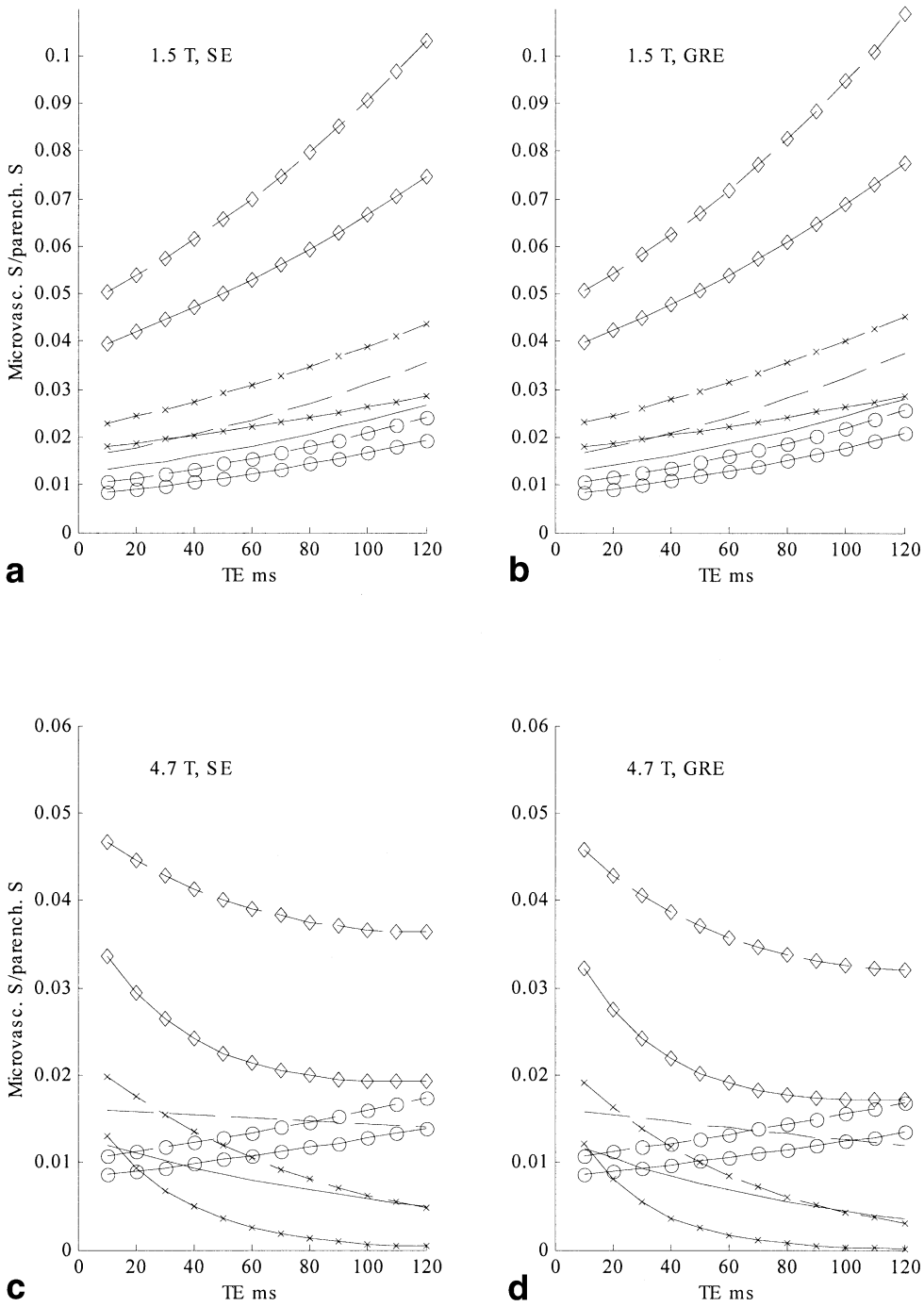

FIG. 6. Estimated fractional signal contribution of the individual microvascular compartments (venules: crosses; capillaries: no markers; arterioles: spheres) and the total microvasculature (diamonds) to the total parenchymal signal at each TE. Baseline activity is shown in solid lines, and neuronal activation in dashed lines. Notice that the intravascular contribution to the total signal increases with TE at low field and reduces with TE at high field, where the signal contribution of the arteries even becomes dominant due to its long TE.

with TE at high field (Fig. 6c and d), thereby rapidly increasing $\Delta S/S$ in veins. As the weight of the venular compartment reduces, the origin of microvascular intravascular BOLD moves toward the capillary area (Fig. 5c and d).

Another important simulation result is that the intravascular contribution to the total parenchymal signal is the same at very short TE at both field strengths studied, while it is about half as large at high field at TE = 100 ms (Figs. 5 and 6). The reason is that signal is dominated by spin density at short TE and is weighted by the effect of transverse relaxation at long TE. Consequently, the intravascular contributions to the BOLD effect are still very large at high field for both SE and GRE at the commonly used TE values of 20–40 ms. The reader will also notice that the total parenchymal BOLD signal change in Fig. 4 is less than the sum of BOLD signal changes calculated for the individual microvessels. The reason is that the tissue volume reduces as the microvascular volume increases (total remains constant). Thus, under these terms, the tissue contribution is negative and reduces the BOLD effect. As the intra- and extravascular BOLD effects are much larger than this reduction, the BOLD effects remain positive (27).

Table 4
Literature Comparison for the Parabolic Constants (in s^{-1}) and Venous Values (at Y = 0.61) of the Relaxation Rates R_2 and R_2^* at 1.5 Tesla†

	A	B	C	R_2(v)	A*	B*	C*	R_2^*(v)
Hct ~ 0.3								
This study	4	0	23	7.5	5.4	0	26	9.4
Spees et al. (14)	3.9	0	55	12.3	4.1	0	88	17.5
Hct ~ 0.4 (normal)								
This study	5	0	21	8.2	6.5	0	25	10.3
Spees et al. (14)	6.5	0	59	15.5	4.9	0	120	23.2
Golay (6 ms, CPMG)	4.6	0	11	6.3				
Wright et al. (17) (6 ms, CPMG)	3.8	0	13	5.8				
Golay (12 ms, CPMG)	4.8	0	15	7.1				
Wright et al. (17) (12 ms, CPMG)	3.9	0	25	7.7				
Golay (24 ms, CPMG)	4.8	0	19	7.7				
Wright et al. (17) (24 ms, CPMG)	4	0	42	10.4				
Li et al. (22), in vitro (human)					7.2	0	35	12.5
Li et al. (22), in vivo (pig)					1.8	0	22	5.1

†Due to sensitivity of the fitting to compensation between B and C constants, a zero B constant was used, as suggested by Wright et al. (17).

To obtain an impression of the validity of these simulations, we calculated the intravascular BOLD effects for some studies in the literature (3,9). Gati et al. (9) measured the absolute signal change (arbitrary units) in veins and parenchyma as a function of TE. Because absolute signal depends on the particular experimental conditions, we can only compare curve shape and relative vein/parenchyma effects. Simulations at 1.5 T using Gati et al.'s (9) acquisition parameters (Fig. 8a–d) show the venous curve (Fig. 8a) flattening off at TE = 80–120 ms. Their experiments showed a maximum at TE = 50–60 ms, which is close to T^*_{2par} at this field strength, indicating some partial voluming with parenchyma. The shape of the parenchymal curves for our simulations (Fig. 8c) and Gati et al.'s (9) data is similar, but the relative change measured for veins versus parenchyma at TE = 60 ms was smaller by about a factor of 4 than in our simulations. Because of partial volume effects and possible extravascular contributions in the in vivo data, any ratio can occur, and comparison is difficult. Comparisons of the data at 4.0 T (9) and 4.7 T (our simulations; Fig. 8b and d) are also not straightforward, especially because transverse relaxation effects tend to go with the square of the field ($4^2 = 16$ vs. $4.7^2 = 22$). Thus, the only general conclusion that can be drawn is from the change in the shape of the curves when going to a

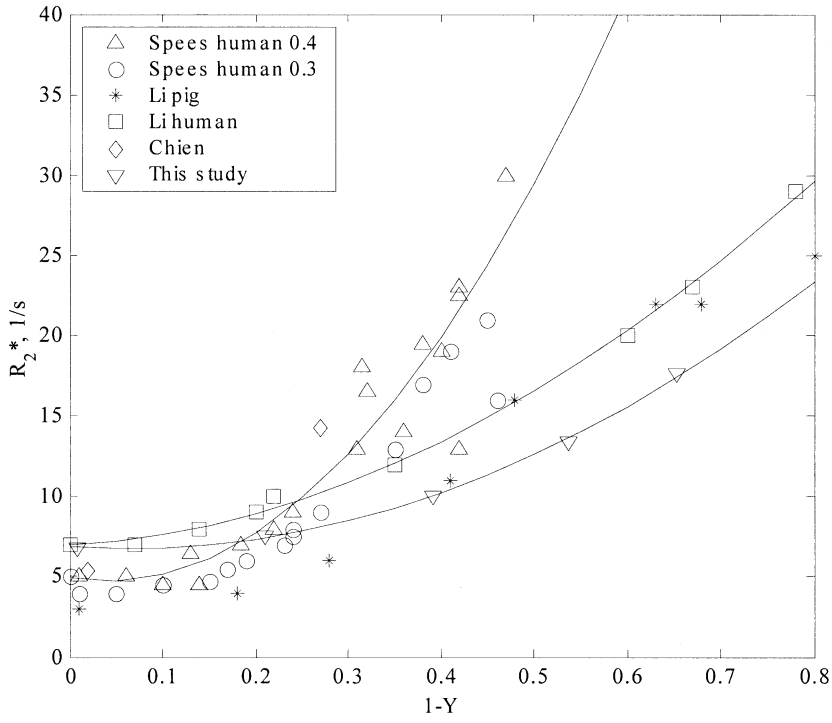

FIG. 7. Comparison of oxygen saturation dependence of R_2^* at 1.5 T with data from the literature. The curves of Li et al. (22) are very comparable, while the data from Spees et al. (14) show much larger relaxation rates, indicating additional field gradient contributions.

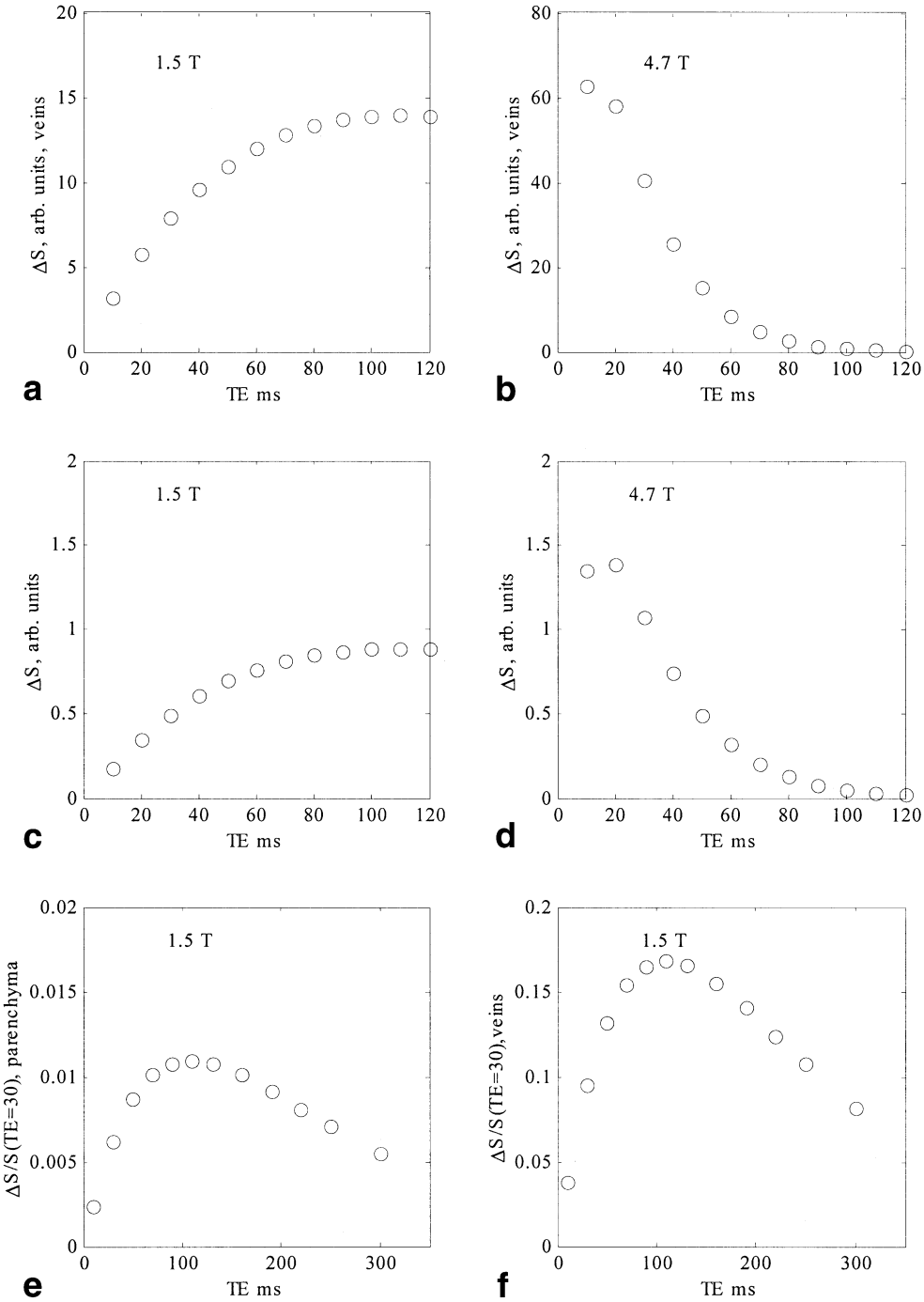

FIG. 8. **a–d:** Estimated intravascular-based BOLD signal changes (arbitrary units) during activation as a function of TE, calculated using the parameters of Gati et al. (9): FA = 20°; TR = 1 s. Data for (**a** and **b**) large veins and (**c** and **d**) parenchyma at 1.5 T and 4.7 T show shapes similar to Gati et al.'s (9) data at 1.5 T and 4.0 T. **e** and **f:** Estimated intravascular-based BOLD signal changes at 1.5 T normalized with respect to signal at TE = 30 ms, similar to the procedure suggested by Hoogenraad et al. (3), and using their parameters (FA = 90°, TR = 6 s). The data for the parenchyma (**e**) show a shape similar to that for the veins (**f**), indicating dominance of the venular contribution.

higher field, which indeed shows a maximum that is moving to lower TE, in agreement with the calculations. Figure 8e and f shows GRE simulations for venous blood and parenchyma with the experimental parameters of Hoogenraad et al. (3). The shapes of the $\Delta S/S(TE = 30$ ms) curves compare favorably. They give maximal $\Delta S/S(TE = 30$ ms) at TE $\approx$ 80 ms, whereas our simulations show it at 100 ms. Our venous $\Delta S/S(TE = 30$ ms) values are approximately double the values of Hoogenraad et al., possibly due to the use of different OER values (0.46 at baseline and 0.32 upon activation) and the higher blood R_2^* values of Li et al. (22). For parenchyma, Hoogenraad et al. (3) reported $\Delta S/S(TE = 30$ ms) of 2–4%, whereas our estimated intravascular R_2^* contribution (Fig. 8f) is about 1%. The difference reflects the effect of microvascular dephasing in extravascular space, previously estimated to about 30% of the net BOLD effect (2,11) and very probably also effects of partial voluming with small veins and CSF, which is unavoidable at present fMRI resolutions. Only if resolution can be improved substantially at high field, and if extravascular dephasing can be minimized (to avoid

CSF contributions from susceptibility changes in neighboring large veins), will it be possible to better focus on parenchymal effects. This is more feasible with the use of SEs than with GREs.

CONCLUSIONS

The SE and GRE transverse relaxation rates, R_2 and R_2^*, of isolated blood were measured as a function of oxygenation, and used to estimate the expected intravascular BOLD effects for typical oxygenation changes during visual activation. The overall conclusion is that, at the field strengths investigated here, quantitative interpretation of the BOLD effects must include the intravascular contributions. Furthermore, the results show that for activation, the intravascular ΔR_2^* is mainly caused by R_2 relaxation changes. These intravascular contributions to the BOLD signal changes in microvasculature are dominated by the venules at all TEs at low field and at short TEs at high field. At longer TEs at high field, the capillary contribution dominates, due to the very short venous transverse relaxation rates. At TE $>$ 70 ms, the intravascular contribution to the relative BOLD change is smaller at high field than at low field, especially for GRE experiments. However, at commonly-used shorter TE values the opposite is the case, which is often not realized. The data also show that both SE and GRE high-field experiments are strongly influenced by partial voluming with veins, raising concerns about the possibility of quantitative interpretation of BOLD effects in typical low-resolution fMRI experiments. However, high-field experiments offer the unique opportunity to increase resolution, thereby allowing partial volume effects to become less of a factor.

REFERENCES

1. Ogawa S, Lee TM, Kay AR, Tank DW. Brain magnetic resonance imaging with contrast dependent on blood oxygenation. Proc Natl Acad Sci USA 1990;87:9868–9872.
2. Boxerman JL, Bandettini PA, Kwong KK, Baker JR, Davis TL, Rosen BR, Weisskoff RM. The intravascular contribution to fMRI signal change: Monte Carlo modeling and diffusion-weighted studies in vivo. Magn Reson Med 1995;34:4–10.
3. Hoogenraad FG, Pouwels PJ, Hofman MB, Reichenbach JR, Sprenger M, Haacke EM. Quantitative differentiation between BOLD models in fMRI. Magn Reson Med 2001;45:233–246.
4. Ogawa S, Menon RS, Tank DW, Kim S-G, Merkle H, Ellerman JM, Ugurbil K. Functional brain mapping by blood oxygenation level-dependent contrast magnetic resonance imaging: a comparison of signal characteristics with a biophysical model. Biophys J 1993;64:803–812.
5. Yablonskiy DA. Quantitation of intrinsic magnetic susceptibility-related effects in a tissue matrix. Phantom study. Magn Reson Med 1998;39:417–428.
6. Hoppel BE, Weisskoff RM, Thulborn KR, Moore JB, Kwong KK, Rosen BR. Measurement of regional blood oxygenation and cerebral hemodynamics. Magn Reson Med 1993;30:715–723.
7. Haacke EM, Hopkins A, Lai S, Buckley P, Friedman L, Meltzer H, Hedera P, Friedland R, Klein S, Thompson L. 2D and 3D high resolution gradient echo functional imaging of the brain: venous contributions to signal in motor cortex studies. NMR Biomed 1994;7:54–62.
8. Frahm J, Merboldt KD, Hanicke W, Kleinschmidt A, Boecker H. Brain or vein—oxygenation or flow? On signal physiology in functional MRI of human brain activation. NMR Biomed 1994;7:45–53.
9. Gati JS, Menon RS, Ugurbil K, Rutt BK. Experimental determination of the BOLD field strength dependence in vessels and tissue. Magn Reson Med 1997;38:296–302.
10. Hoogenraad FG, Hofman MB, Pouwels PJ, Reichenbach JR, Rombouts SA, Haacke EM. Sub-millimeter fMRI at 1.5 Tesla: correlation of high resolution with low resolution measurements. J Magn Reson Imaging 1999;9:475–482.
11. Song AW, Wong EC, Tan SG, Hyde JS. Diffusion weighted fMRI at 1.5 T. Magn Reson Med 1996;35:155–158.
12. Thulborn KR, Waterton JC, Matthews PM, Radda GK. Oxygenation dependence of the transverse relaxation time of water protons in whole blood at high field. Biochim Biophys Acta 1982;714:265–270.
13. Oja JM, Gillen JS, Kauppinen RA, Kraut M, van Zijl PC. Determination of oxygen extraction ratios by magnetic resonance imaging. J Cereb Blood Flow Metab 1999;19:1289–1295.
14. Spees WM, Yablonskiy DA, Oswood MC, Ackerman JJ. Water proton MR properties of human blood at 1.5 Tesla: magnetic susceptibility, T1, T2, T2*, and non-Lorentzian signal behavior. Magn Reson Med 2001; 45:533–542.
15. Gomori JM, Grossman RI, Yo-Ip C, Asakura T. NMR relaxation times of blood: dependence on field strength, oxidation state, and cell integrity. J Comput Assist Tomogr 1987;11:684–690.
16. Bryant RG, Marill K, Blackmore C, Francis C. Magnetic relaxation in blood and blood clots. Magn Reson Med 1990;13:133–144.
17. Wright GA, Hu BS, Macovski A. Estimating oxygen saturation of blood in vivo with MR imaging at 1.5T. J Magn Reson Imaging 1991;1:275–283.
18. Matwiyoff NA, Gasparovic GM. Comments on bulk magnetic susceptibility frequency shifts in cell suspensions. NMR Biomed 1994;7:195–202.
19. Chien D, Levin DL, Anderson CM. MR gradient echo imaging of intravascular blood oxygenation: T2* determination in the presence of flow. Magn Reson Med 1994;32:540–545.
20. Meyer M-E, Yu O, Eclancher B, Grucker D, Chambron J. NMR relaxation rates and blood oxygenation level. Magn Reson Med 1995;34: 234–241.
21. Gillis P, Peto S, Moiny F, Mispelter J, Cuenod CA. Proton transverse nuclear magnetic relaxation in oxidized blood: a numerical approach. Magn Reson Med 1995;33:93–100.
22. Li D, Wang Y, Waight DJ. Blood oxygen saturation assessment in vivo using T2* estimation. Magn Reson Med 1998;39:685–690.
23. van Zijl PC, Eleff SM, Ulatowski JA, Oja JM, Ulug AM, Traystman RJ, Kauppinen RA. Quantitative assessment of blood flow, blood volume and blood oxygenation effects in functional magnetic resonance imaging. Nat Med 1998;4:159–167.
24. Golay X, Silvennoinen MJ, Zhou J, Clingman CS, Kauppinen RA, Pekar JJ, van Zijl PC. Measurement of tissue oxygen extraction ratios from venous blood T2: increased precision and validation of principle. Magn Reson Med 2001;46:282–291.
25. Leenders KL, Perani D, Lammertsma AA, et al. Cerebral blood flow, blood volume and oxygen utilization. Normal values and effect of age. Brain 1990;113:27–47.
26. Phelps ME, Huang SC, Hoffman EJ, Kuhl DE. Validation of tomographic measurement of cerebral blood volume with C11-labeled carboxyhemoglobin. J Nucl Med 1979;20:328–334.
27. Lu H, Golay X, van Zijl PCM. Inter-voxel heterogeneity of event-related fMRI responses as a function of T1-weighting. Neuroimage 2002;17: 943–955.
28. Zhou J, van Zijl PC. Perfusion imaging using FAIR with a short predelay. Magn Reson Med 1999;41:1099–1107.
29. Takagi H, Shapiro K, Marmarou A, Wisoff H. Microgravimetric analysis of human brain tissue: correlation with computerized tomography scanning. J Neurosurg 1981;54:797–801.
30. Herscovitch P, Raichle ME. What is the correct value for the brain-blood partition coefficient for water? J Cereb Blood Flow Metab 1985; 5:65–69.
31. Sharan M, Jones MDJ, Koehler RC, Traystman RJ, Popel AS. A compartmental model for oxygen transport in brain microcirculation. Ann Biomed Engin 1989;17:13–38.
32. Fox PT, Raichle ME. Focal physiological uncoupling of cerebral blood flow and oxidative metabolism during somatosensory stimulation in human subjects. Proc Natl Acad Sci USA 1986;83:1140–1144.

33. Grubb Jr RL, Raichle ME, Eichling JO, Ter-Pogossian MM. The effects of changes in PaCO2 on cerebral blood volume, blood flow, and vascular mean transit time. Stroke 1974;5:630–639.
34. Zhou J, Golay X, van Zijl PC, Silvennoinen MJ, Kauppinen R, Pekar J, Kraut M. Inverse T2 contrast at 1.5 Tesla between gray matter and white matter in the occipital lobe of normal adult human brain. Magn Reson Med 2001;46:401–406.
35. Ulatowski JA, Oja JM, Suarez JI, Kauppinen RA, Traystman RJ, van Zijl PC. In vivo determination of absolute cerebral blood volume using hemoglobin as a natural contrast agent: an MRI study using altered arterial carbon dioxide tension. J Cereb Blood Flow Metab 1999;19:809–817.
36. Brooks RA, Di Chiro G. Magnetic resonance imaging of stationary blood: a review. Med Phys 1987;14:903–913.
37. Lee SP, Silva AC, Ugurbil K, Kim SG. Diffusion-weighted spin-echo fMRI at 9.4 T: microvascular/tissue contribution to BOLD signal changes. Magn Reson Med 1999;42:919–928.
38. Zhu XH, Chen W. Observed BOLD effects on cerebral metabolite resonances in human visual cortex during visual stimulation: a functional 1H MRS study at 4 T. Magn Reson Med 2001;46:841–847.
39. Morariu VV, Pop VI, Popescu O, Benga G. Effects of temperature and pH on the water exchange through erythrocyte membranes: nuclear magnetic resonance studies. J Membr Biol 1981;62:1–5.
40. Barth M, Moser E. Proton NMR relaxation times of human blood samples at 1.5 T and implications for functional MRI. Cell Mol Biol (Noisy-le-Grand) 1997;43:783–791.